

Revealing building operating carbon dynamics for multiple cities

Winston Yap¹, Abraham Noah Wu¹, Clayton Miller², Filip Biljecki^{1,3,*}

¹*Department of Architecture, National University of Singapore, Singapore*

²*Department of the Built Environment, National University of Singapore, Singapore*

³*Department of Real Estate, National University of Singapore, Singapore*

Abstract

Achieving carbon neutrality is a critical yet elusive goal for many cities, hindered by limited understanding of the relationship between building emissions and their surroundings. To address this challenge, we present a generalizable open science framework that integrates building energy consumption data, multi-modal geospatial inputs, and graph deep learning to quantify building operating emissions and their links to urban form and socioeconomic factors. Applying this approach to five cities with diverse climates and planning contexts—Melbourne, New York City (Manhattan), Seattle, Singapore, and Washington DC—we demonstrate that our models explain 78.4% of the variation in building operating carbon emissions across cities, achieving state-of-the-art accuracy for urban-scale energy modeling. Our findings reveal strong connections between a city’s planning history and its building carbon profile, alongside stark inequalities where wealthier areas often exhibit the highest per capita emissions. Additionally, the relationship between urban density and building emissions is complex and city-specific, with emissions extending beyond dense urban cores into suburban areas. To design effective decarbonization strategies, cities must consider how their planning histories, urban layouts, and economic conditions shape current emission patterns.

Keywords: Climate Change, City Science, Machine Learning, GeoAI, Urban Analytics

Main

Cities are pivotal in the global transition towards a sustainable urban future [1]. To meet Intergovernmental Panel on Climate Change (IPCC) targets, urgent reforms are imperative for the built environment, which currently exhausts the largest sectoral share of global emissions [2, 3]. A collective global initiative is underway to foster a more sustainable and climate-resilient urban future across cities with over 37% of cities worldwide committing to net-zero pledges [4, 5]. These pledges are backed by multi-sectoral plans to curtail building energy consumption by mandating energy-efficient building standards, promoting clean energy generation, and encouraging sustainable energy consumption behavior. Several countries, including the US, China, Japan, Australia, and Türkiye, have tightened national building regulations to mandate zero-energy performance for both new and existing buildings [6]. While promising, current estimates reveal an insufficient pace and scale in the global clean energy transition to align the building sector with Paris Climate targets [7]. Notably, nearly half of cities worldwide continue to lack identifiable emission mitigation targets, and only 3% of cities with net-zero

*Corresponding author

Email address: filipt@nus.edu.sg (Filip Biljecki)

commitments meet the starting criteria outlined by the United Nations Framework Convention on Climate Change (UNFCCC) [5]. The urgent need for a livable and sustainable future necessitates rapid and extensive changes across all sectors and systems [8].

Despite extensive planning efforts, many cities struggle to decarbonize their built environments, largely due to a limited understanding of how buildings interact with their urban contexts [9, 10]. While numerous studies have investigated the relationship between urbanization and carbon emissions at the city scale, these analyses often emphasize broader urban trends rather than the fine-grained spatial heterogeneity that exists within cities. For instance, [11] observed that population growth in large cities drives emissions increases, albeit with diminishing returns to scale. Similarly, [12] highlighted how compact urban planning and advanced energy technologies can yield economies of scale in energy savings. At the metropolitan scale, studies on street networks suggest that many cities are locked into unsustainable development pathways, requiring drastic action to avoid costly lock-ins and deviate from the status quo [13]. The impacts of urban sprawl on urban-induced warming also vary significantly across regions [14, 15]. However, major data gaps persist within cities, limiting policymakers' ability to assess policy impacts, monitor progress, and implement informed adjustments to reduce emissions and build climate resilience [16, 17, 18].

Urban building energy modeling (UBEM) has significantly advanced our understanding of spatial variability in building energy use at urban scales [19]. Notably, [20] explored end-use energy patterns by building function, while recent studies have integrated human mobility data to refine occupancy and energy use estimates at high spatial resolutions [21, 22]. Notwithstanding, city-scale UBEM still confronts key limitations. Models often rely on generalized building archetypes, which can lead to significant errors at finer spatial scales [19], and they tend to be location-specific, limiting their transferability across cities with different data inputs and building typologies [23].

To address these challenges, recent efforts have increasingly turned to machine learning methods [24]. For instance, [25] developed a multi-stage pipeline that leverages aerial imagery and building footprints to predict residential energy consumption in American neighborhoods. Building on this, [26] applied deep learning to combine satellite imagery with urban occupancy data for estimating building energy use in New York City. Extending this line of work, recent innovations have highlighted the potential of urban visual intelligence, a framework that interprets city sensing through images, for building energy prediction, with studies showing that models using street view imagery (SVI) can achieve state-of-the-art performance [27, 28, 29, 30]. More recent studies have explored multi-modal approaches that integrate land surface temperature, street view and aerial imagery, and building footprints to predict the energy efficiency of buildings in the United Kingdom [31, 32].

To the best of our knowledge, prior studies on urban-scale building energy studies have typically examined individual cities or specific building types, limiting cross-city insights. Many depend on proprietary inputs such as Google Street View, mobility traces, or high-resolution imagery that are often inaccessible in developing cities. The emergence of high-quality open urban datasets [33, 34] presents new opportunities for scalable, bottom-up modeling of urban building energy emissions. Our study introduces a highly granular, transferable framework for predicting urban-scale building operating emissions using open and widely available multi-modal datasets. We encode spatial relationships between buildings and their surroundings through a rich set of features, including urban form, infrastructure, population density, and urban services through a deep graph model that captures the non-linear, localized variations in emissions across five cities—Melbourne, NYC (Manhattan), Seattle, Singapore, and

Washington DC

Building carbon emission consists of operational carbon [35] and embodied carbon [36]. Operational emissions depend on building function, climate, form, materials, and operating practices, with Heating, Ventilation, and Air Conditioning (HVAC) systems, lighting, and plug loads as the primary sources. We focus on estimating operational emissions from buildings, which typically dominate a building’s life-cycle footprint [37]. However, in certain scenarios, embodied carbon may gain prominence, influenced by factors like building lifespan, climatic conditions, and regulations, alongside low-carbon electricity grids [38].

Our analysis reveals how planning history, urban form, and economic activity interact to shape heterogeneous emissions patterns across cities. These findings provide path-dependent insights into the developmental trajectories of other urban areas. Additionally, we examine the complex relationship between urban density and emissions within cities by incorporating local climate zones, urban heat island intensity, and real GDP per capita.

Our study emphasizes the transformative potential of open science and large-scale urban sensing can guide equitable decarbonization pathways and contribute to achieving sustainable urban transitions in alignment with the Sustainable Development Goals (SDGs): Reduced Inequalities (SDG10), Sustainable Cities and Communities (SDG11), and Climate Action (SDG13).

Results

We implement our task for 595,173 buildings across five cities worldwide in diverse climatic regions—Melbourne, NYC (Manhattan), Seattle, Singapore, and Washington DC. Due to resource limitations, our analysis in NYC focuses on the Manhattan borough, which is one of the most urbanized and densely populated areas in the United States.

Each city has a different climate and built typology which presents unique challenges for city-scale building energy modeling. Singapore, a densely populated tropical city with high temperatures and humidity, uses most of its energy for cooling buildings, placing significant demands on systems designed to maintain indoor thermal comfort. Its building stock predominantly consists of high-rise residential structures, which experience significant temperature variations due to urban heat island effects. Meanwhile, Melbourne and Seattle are coastal cities with temperate Mediterranean climates, providing a unique opportunity to analyze year-round energy consumption for heating and cooling across various building types in urban and suburban settings. NYC is an East Coast seaport city located in the Atlantic Ocean coastal zone of the eastern United States, characterized by a temperate continental climate. Manhattan features a highly dense mix of residential and commercial buildings. This dense urban form increases its vulnerability to climate change with exacerbating effects from a widespread urban heat island effect. Washington DC has a humid subtropical climate with sprawling suburbs and heightened urban heat risk.

To create a detailed contextual representation of each building and its surroundings, we gather and harmonize a variety of open urban data sources, as detailed in Table I. Figure 1 offers a schematic representation of the data sources we used and the experimental setup of our study.

Graph neural networks utilize message-passing mechanisms to acquire contextual information from their neighboring nodes. In our case, each building is represented by a single node which aggregates information from its surrounding spatial entities such as nearby street or neighboring buildings. Figure 2 shows the graph generation and model training process.

Table 1: Description of open data characteristics and building carbon stock across cities.

Cities	Availability (%) ¹	#Bldgs	#SVI	#Satellite Images ²	#POIs	# Streets	Total Em. ($MtCO_2$)	Net Zero ³
Melbourne	4.24	111,763	162,545	34,341	29,235	224,646	3.86	2040
NYC (Manhattan) ⁴	17.66	45,164	24,926	14,451	18,606	24,444	12.25	2040
Seattle	1.30	193,314	95,006	26,715	13,020	153,806	4.76	2050
Singapore	7.87	105,911	49,736	66,660	29,235	225,730	19.46	2050
Washington DC	1.89	139,021	195,985	13,870	7,991	104,868	9.42	2045

Bldgs—Buildings; SVI—Street View Images; Em.—Emission; POIs—Points of Interests.

¹ Percentage of buildings with reported energy data relative to the total number of buildings highlights data scarcity and drives our use of deep learning for city-scale building energy modeling. Table S2 offers a detailed breakdown of emission statistics by building type.

² Satellite images are provided by Mapbox at 512 by 512 pixels resolution at zoom level 19 (approximately 0.149 meters per pixel at the equator).

³ Target years signify each city’s commitment to lowering carbon emissions to a point where the release of greenhouse gases into the atmosphere is balanced by removal or offset methods.

⁴ New York City has more than one million buildings. Due to limited resources, we focus on Manhattan borough which accounts for approximately 40% of building carbon emission for New York City: [NYC Decarbonization Compass](#).

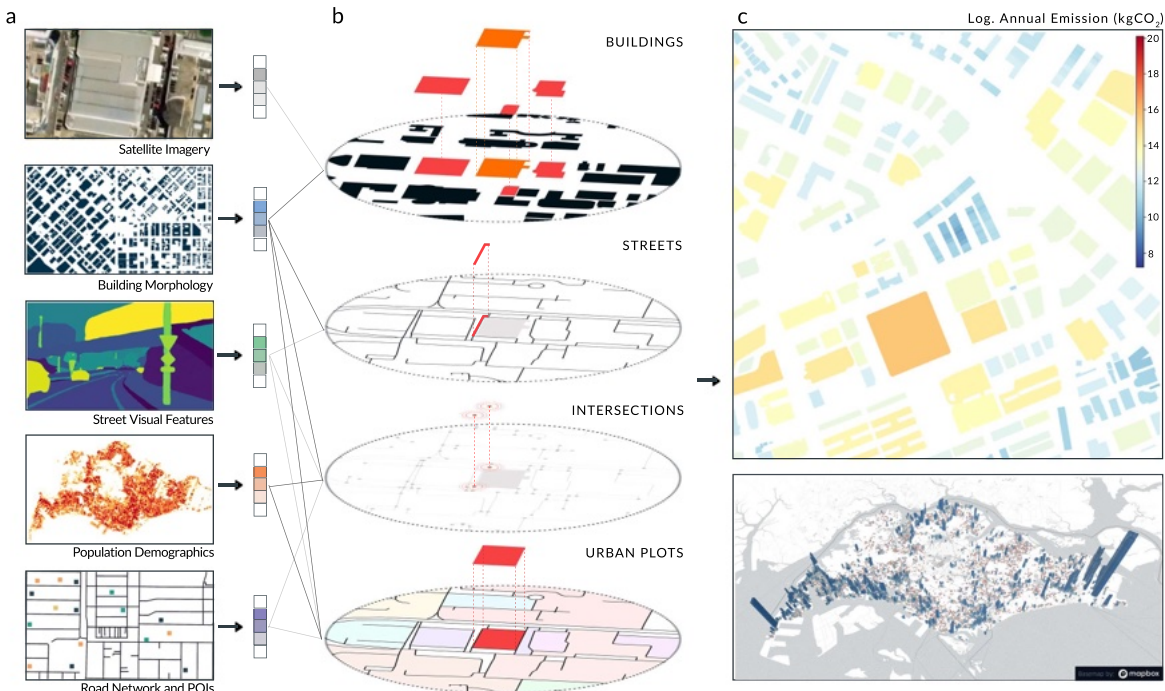


Figure 1: Schematic illustration of the data and workflow. A) Multi-modal data, including satellite imagery, building footprints from OpenStreetMap, street view images, population demographics, and urban points of interest, are harmonized to create feature-rich urban embeddings [59]. B) Our method involves constructing one comprehensive city-scale graph for each city, encompassing all nodes and edge information. For training and validation, computational subgraphs are generated that are centered on each building. These computational subgraphs capture the connection between buildings and their urban context. For example, a building is connected to its nearest urban elements, such as neighboring buildings, urban plot, and nearest street. C) Leveraging openly available building energy data as ground truth, we employ heterogeneous graph neural networks to capture the nonlinear relationship between building emissions and their surrounding urban context. We then apply these models to generate detailed maps of the carbon profile for the built environment across entire cities. Sources of the data samples: (c) OpenStreetMap contributors, Mapillary, Meta. Basemap: [OpenStreetMap](#) and [Mapbox](#).

Planning History and Carbon Profiles of Cities

Carbon profile of cities reflect their historical planning context, suggesting path-dependent insights into emission outcomes. Here we relate planning context to the spatial distribution of building operating emissions and urban form factors (accounting for individual building and plot level characteristics). Figure 3A illustrates the cumulative distribution of predicted build-

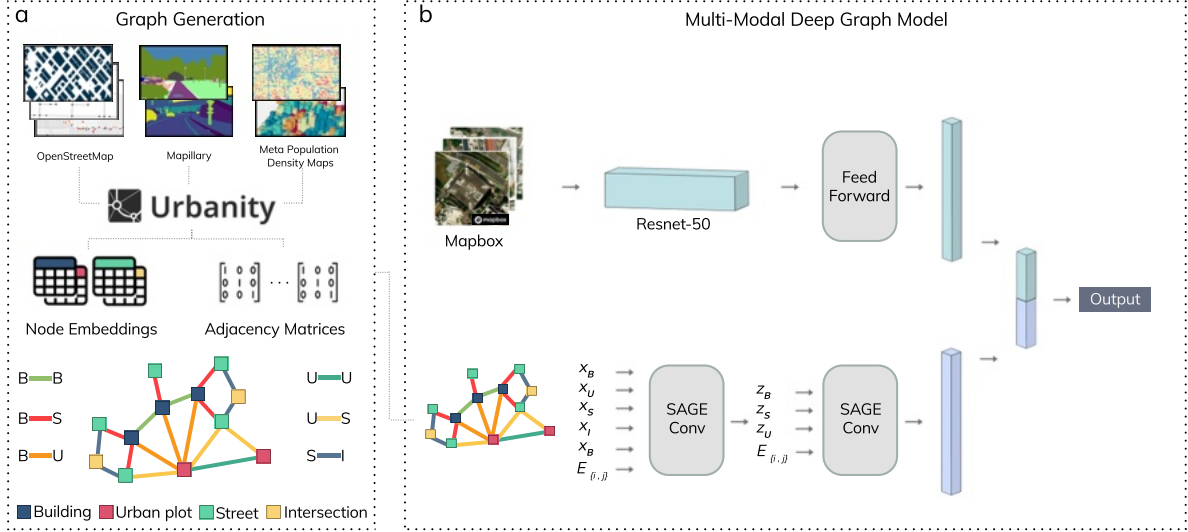


Figure 2: Graph generation pipeline and model training process. A) Node embeddings and adjacency matrices are automatically generated using the Urbanity Python package. For instance, building features are derived from morphological metrics such as area, shape index, and complexity (refer to SI Appendix, Supplementary Table 1 for a detailed list of indicators). We use the Urbanity package to construct neighbor links by connecting each building’s centroid to its three nearest neighbors. The heterogeneous urban graph comprises four node categories—buildings, urban plots, streets, and intersections—and features six types of edges: 1) building-to-building, 2) building-to-urban plot, 3) building-to-street, 4) plot-to-plot, 5) plot-to-street, and 6) street-to-intersection. These edges reflect the spatial relationships among urban entities, such as buildings contained within urban plots and streets connected to intersections. B) The model integrates multi-modal information in two steps. First, an image feature extraction backbone like ResNet-50 obtains visual features from satellite images centered on building centroids. Concurrently, the heterogeneous deep graph module receives node embeddings and adjacency matrices as input. To account for node heterogeneity, different graph convolutional modules are applied for each edge types. The first graph convolutional layer aggregates features from immediate neighbors, while the second layer captures information from two-hop neighborhoods. Sources of the data samples: (c) OpenStreetMap contributors, Mapillary, Meta. Satellite images: [Mapbox](#).

ing emissions relative to footprint area across all buildings in each city. In cities like Seattle and Washington DC, characterized by a history of low-rise development and urban sprawl, small buildings dominate carbon emissions. Conversely, Melbourne’s emissions scale proportionally with building size, reflecting its gradual suburban-to-urban transition over the past century. In contrast, Singapore and New York City (Manhattan) concentrate most emissions in their largest buildings. Notably, the top decile of buildings in New York City contributes more than half of total building emissions, a finding consistent with external reports that nearly half of New York City’s building emissions originate from just 2% of its buildings [39]. Our findings suggest that decarbonization efforts, such as data reporting and retrofitting, must focus on the building sizes that contribute most to emissions in each city. A context-sensitive, targeted approach will maximize resource efficiency and accelerate progress toward decarbonization goals.

To support understanding of how urban form influences citywide emissions, we quantified emissions across local climate zone (LCZ) categories. Figure 3B reveals a consistent pattern: compact high-rise and heavy industrial zones exhibit significantly higher average emissions, often exceeding those of low-rise areas by an order of magnitude or more (e.g., in Melbourne, emissions are over 10 times higher). However, substantial variation within each LCZ category underscores the importance of targeting top emitters. In contrast, compact low-rise zones display markedly lower average emissions per plot, highlighting the role of local characteristics in

shaping emission profiles and the need for tailored decarbonization strategies.

Our findings align with the spatial distribution of building carbon emissions in each city. From Figure 3C, we observe that emissions are highest on average in urban cores and follow a far-right-tailed distribution in cities with significant suburban development. A notable exception is Singapore, where emissions exhibit a balanced, normal distribution, concentrated around the urban periphery. This unique pattern aligns with Singapore’s polycentric development model and diversified land use strategy, emphasizing the influence of urban planning on emission distributions.

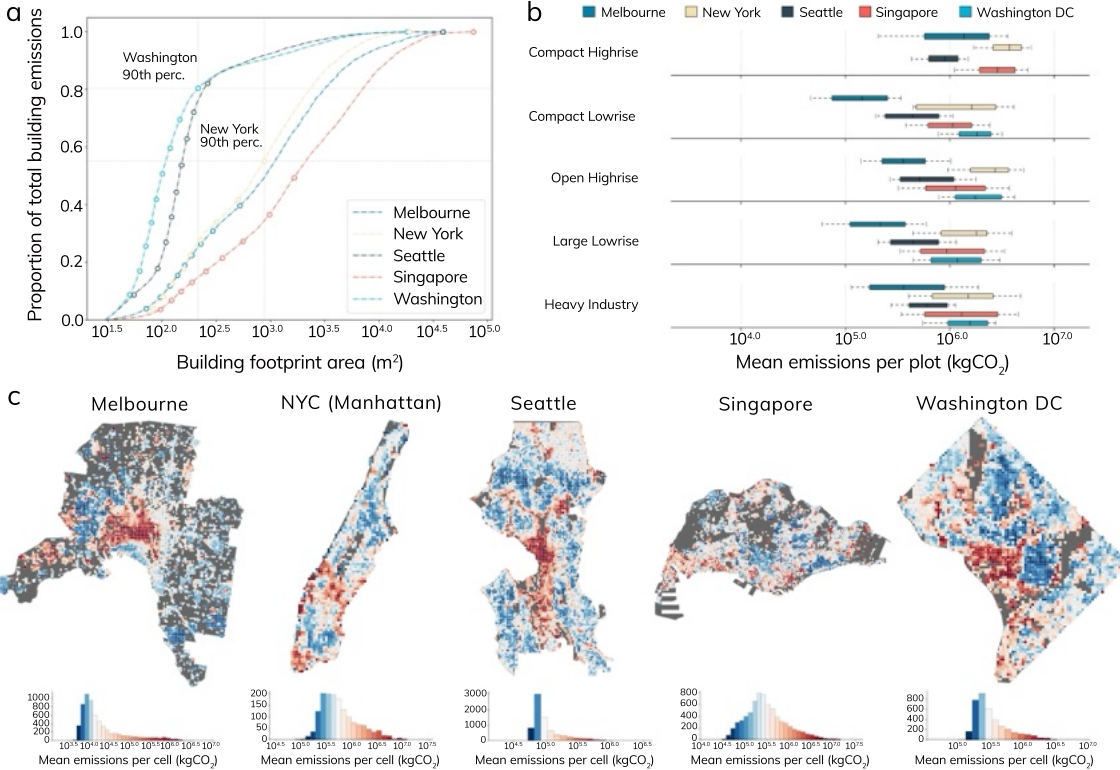


Figure 3: (A) Cumulative distribution of total predicted building operating carbon emissions and its relationship with increasing building footprint size. (B) The grouped plot shows average building operational carbon emissions across local climate zones, omitting estimates with fewer than 30 samples. Sample sizes for each zone and city are as follows: Compact Highrise (Melbourne=409; NYC=1,299; Seattle=471; Singapore=76), Compact Lowrise (Melbourne=244; NYC=42; Seattle=220; Singapore=639; Washington DC=971), Open Highrise (Melbourne=331; NYC=330; Seattle=60; Singapore=5,083; Washington DC=83), Large Lowrise (Melbourne=2,866; NYC=51; Seattle=1,377; Singapore=334; Washington DC=631), and Heavy Industry (Melbourne=153; NYC=115; Seattle=141; Singapore=1,526; Washington DC=50). Each bar in the plot is color-coded by city, with the centerline indicating the median and whiskers representing the 10th and 90th percentiles. (C) Spatial distribution of predicted mean building carbon emissions across cities aggregated across 250-meter grid cells.

Urban Density and Building Emissions

Urban density and building carbon emissions have a complex relationship. Although compact, high-density development is often associated with lower emissions, some studies also highlight increased energy consumption due to urban heat island effects in densely built areas. From Figure 4A, we observe a consistent, scale-invariant negative relationship between emissions per unit area and larger, more complex building footprints. In addition, this relationship

remains consistent even after accounting for building verticality. Specifically, we observe a significant negative correlation between building volume (height multiplied by footprint area) and emissions per unit area across all cities studied. For example, the correlation coefficients are as follows: Melbourne ($r = -0.116$), NYC–Manhattan ($r = -0.470$), Seattle ($r = -0.822$), Singapore ($r = -0.475$), and Washington DC ($r = -0.793$). These results suggest that taller buildings—with greater volume—tend to exhibit lower emissions per unit area, likely due to differences in operational energy demands and the technical systems employed. The varying strength of this relationship across cities indicates that local building design, usage patterns, and energy infrastructures play a key role in shaping emissions from tall buildings. This finding indicates that emission intensity does not grow proportionally with building size and complexity, suggesting economies of scale and significant carbon savings in bigger buildings.

Our results also imply that reducing building sizes without considering land-use intensity may not effectively lower overall carbon emissions; in fact, doing so could shift building functions elsewhere and potentially increase emissions across the broader built environment. Furthermore, as higher population density and urbanization trends push toward more high-rise construction in cities, it is crucial for cities to monitor the energy loads of their high-rise building stock.

At the urban scale, Figure 4B illustrates the complex, city-specific relationship between building footprint coverage and average building emissions, primarily influenced by urban form compactness. In cities with significant suburban development—such as Melbourne, Seattle, and Washington DC—higher overall building footprint coverage typically comes from fewer but larger structures, making building height a critical factor in determining emissions. Our results suggest that, in Melbourne, increases in building height outpace increases in footprint area, causing larger buildings to have higher emissions. However, in Seattle and Washington, DC, larger footprints are not matched by comparable increases in height, resulting in lower average carbon emissions per building. In contrast, compact cities like Singapore and Manhattan maintain consistently high building heights regardless of footprint coverage.

Across all cities, we observe a consistent negative association between population density and average building emissions. This pattern aligns with previous studies reporting a negative correlation between population density and building emissions [12]. Densely populated areas often contain more, but smaller, housing units that require less energy for heating, cooling, and maintenance, leading to lower per-building emissions [40]. Moreover, population density has been shown to more strongly affect on-road transportation emissions than building emissions [41]. Additionally, LCZ diversity (see Methods for computation details) shows a significant positive relationship with emissions in Melbourne and Seattle. This finding makes intuitive sense, as suburban areas with homogeneous LCZ patterns tend to have buildings with lower emissions, whereas areas with greater LCZ diversity usually contain buildings with more varied functions and a wider range of emissions. These findings align with the positive relationship between urban heat island intensity and emissions, further confirming that denser built-up areas correspond to higher average emissions for buildings.

Overall, the relationship between urban density and building emissions is multifaceted, shaped by each city’s unique development patterns. Our findings highlight the need to extend decarbonization efforts beyond dense urban cores to include suburban areas, especially in cities with extensive suburban development.

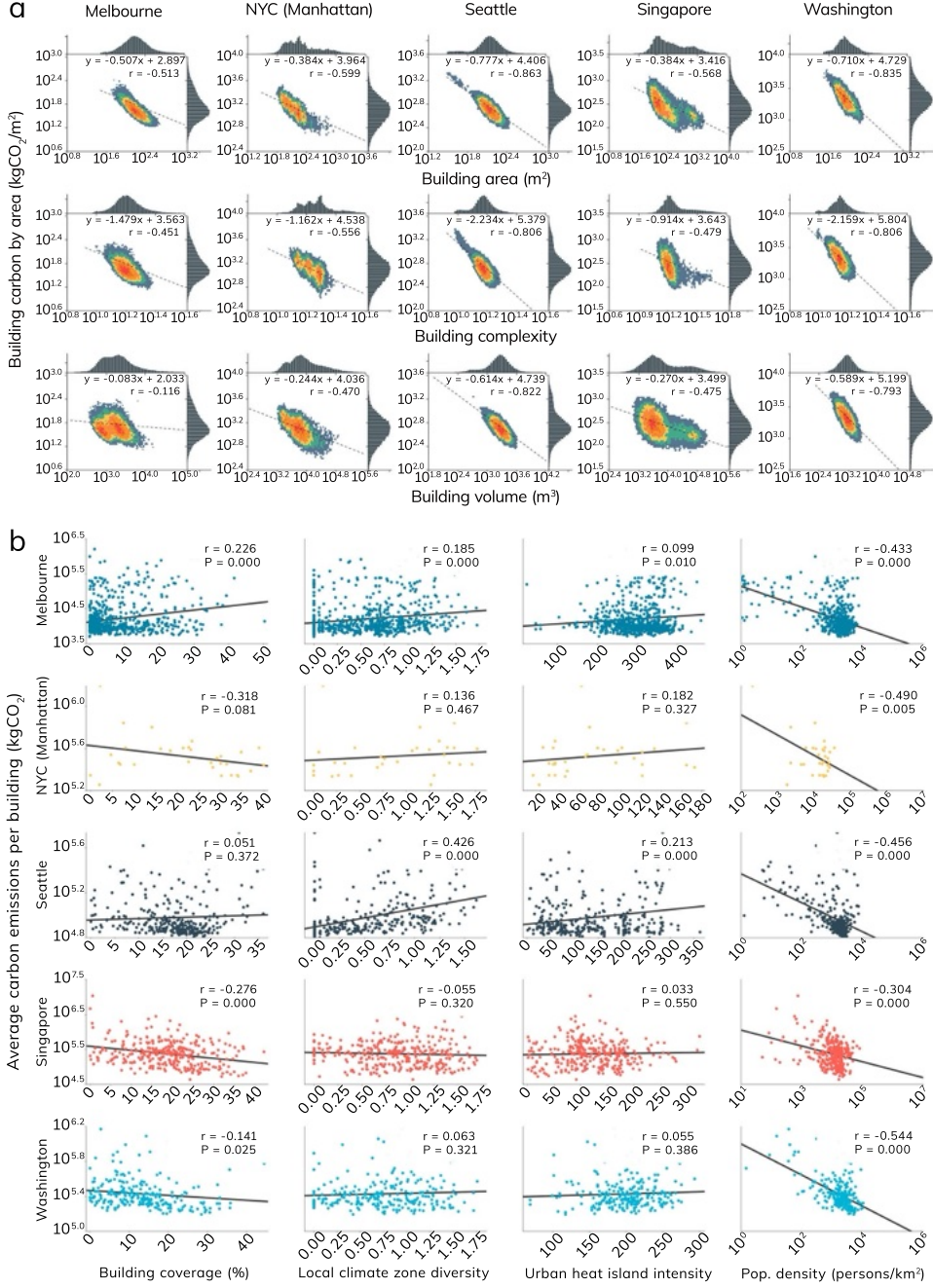


Figure 4: Relationship between urban density, microclimatic conditions, and building emissions. (A) Economies of scale are observed across all cities with building emissions per unit area decreasing with increasing building footprint area and shape complexity. The relationship between emissions per unit area and building height provides insights into how building footprint area changes with height in cities such as Melbourne, Seattle, and Washington DC. (B) We report the two-sided Pearson correlation coefficients and corresponding p-values between building emissions and four key urban variables: building coverage, local climate zone diversity, population density, and urban heat island intensity. While population density consistently shows a negative correlation with average building emissions, the relationship between building density and emissions is more complex. This variability is largely influenced by the unique urban form of each city.

Equitable Decarbonization

Decarbonization efforts must equitably benefit all societal groups. To assess how the burden of decarbonization varies across communities, we map the relationship between real GDP

per capita [42] and predicted per capita building operating emissions across cities. While earlier nighttime light-derived GDP estimates suffered from considerable noise and uncertainty, recent satellite programs provide higher-resolution estimates which have shown strong association with human activity [43] [44]. Collectively, these advancements demonstrate that integrating high-resolution nighttime lights with detailed population estimates effectively captures local socioeconomic variability and gridded GDP datasets are increasingly employed in diverse urban research domains.

Figure 5A shows a consistent trend across all cities where building emissions per capita rises with an increase in real GDP per capita. In Melbourne, suburban development contributes to higher per capita emissions in areas with lower real GDP per capita. This aligns with the dominance of detached single-family homes in the suburbs, one of the least energy- and resource-efficient building types. In addition, building emissions are markedly higher (more than ten times) for the wealthiest urban areas (90th and 100th percentile) for all cities.

Figure 5B reveal the complex relationship between urban economic activity and building emissions. Areas with both high real GDP and high emissions per capita are typically concentrated in urban cores, though this pattern is not strictly linear. High-emission, low-GDP areas and low-emission, high-GDP areas also constitute significant portions of cities, highlighting substantial heterogeneity in the spatial distribution of emissions. This heterogeneity between urban economic activity and emissions highlights the need for spatially tailored supply-side policies, such as carbon taxes, to prevent imposing disproportionate economic burdens on vulnerable communities.

Decarbonization will affect high and low income communities in different cities to varying degrees. To better understand the extent, Figure 5C shows the relationship between cumulative building emissions and real GDP per capita deciles. In an egalitarian situation where emissions are distributed uniformly across the population, cumulative emissions will rise in tandem with real GDP per capita. However, we observe that urban areas with lower real GDP per capita account for a large percentage of the total emission for cities like Melbourne, Seattle, and Washington DC. For example, urban areas consisting of the bottom 20 percentile of real GDP per capita comprise 60% of total emissions in Melbourne. These emissions are largely driven by educational and civic buildings—many of which are large facilities serving institutional functions. Although such buildings contribute substantially to citywide emissions, their impact is not directly captured through conventional measures of economic activity. Our finding shows that on the whole, decarbonization policies would mostly affect urban areas with lower real GDP per capita and it is important to consider measures to reduce economic burden on vulnerable communities.

Discussion

Our study introduces a multi-city, graph deep learning-based framework to understand the complex and spatially heterogeneous building carbon profile of cities. Understanding the underlying drivers of building emissions is not only critical to support actionable and equitable decarbonization strategies but also reveals the potential for transferable, path-dependent insights for other cities.

In line with previous research [45, 12], we find that urban density plays a significant role in shaping building emissions across cities. Higher population density, larger building footprints, and greater building volumes are associated with lower emissions per unit of built-up area, reflecting economies of scale in energy use. Our analysis reveals that density-related efficiencies

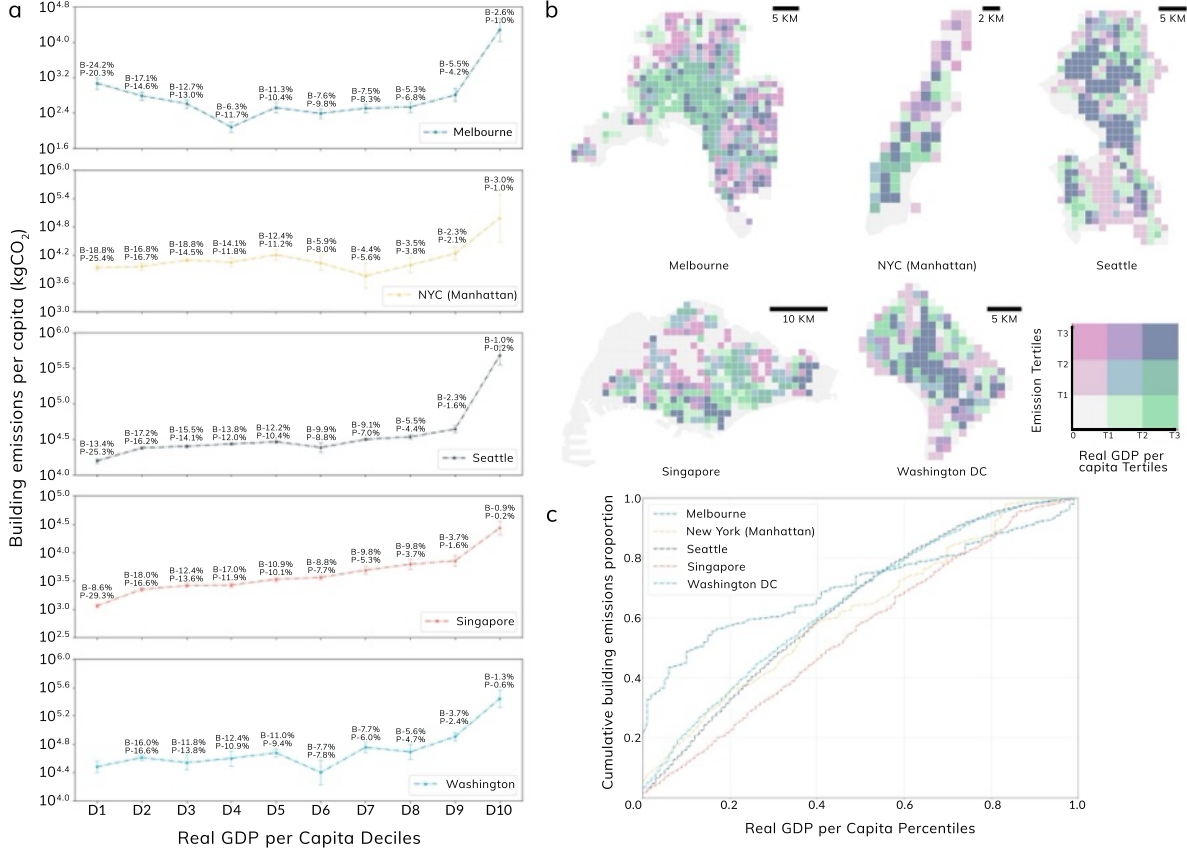


Figure 5: Relationship between income levels and building emissions. (A) The decile plot shows real GDP per capita against building emissions per capita, with markers indicating the mean and error bars representing the one standard error range for each decile. Each city is divided into equal-sized bins with the following bin counts: Melbourne (46), NYC (6), Seattle (27), Singapore (30), and Washington DC (19). Deciles are annotated with the percentage of buildings (B%) and population (P%) within each city. (B) Spatial distribution of real GDP per capita [42] and building emissions per capita, aggregated at 1 km by 1 km grid cells. Grids without population are excluded, and marker sizes reflect the estimated population [64] within each cell. (C) Cumulative relationship between building emissions and real GDP per capita.

manifests differently across geographies, particularly when accounting for additional contextual factors like the composition and arrangement of building typologies. In cities like Singapore, New York City (Manhattan), and Washington, DC, areas with higher building coverage show clear emissions savings, as energy efficiencies from scale reduce the average emissions of buildings in high-density zones. Yet in Melbourne and Seattle, areas with higher building coverage exhibit elevated emissions due to local climate zone (LCZ) diversity and urban heat island (UHI) intensity factors, suggesting that micro-climate factors can offset the gains from density. These findings highlight that high-density development is not a one-size-fits-all solution and that the combination of contextual factors like building typology mix and arrangement creates complex emissions patterns that cannot be addressed through density-based planning alone. Instead, effective emissions mitigation in dense urban environments requires a nuanced, place-based approach that co-optimize compactness and climate-sensitive urban design.

Our findings build on prior research highlighting the significant contribution of suburban emissions to overall urban carbon footprints [46]. Specifically, we show that suburban building emissions can, in many cases, rival those of urban cores, creating substantial carbon hotspots that are often overlooked in decarbonization planning. Moreover, emissions do not scale lin-

early with economic activity. Several high-emission areas exhibit relatively low real GDP per capita, pointing to underlying drivers such as inefficient building practices, outdated infrastructure, poor land-use planning or functional mismatches, and unsustainable consumption patterns. This disconnect between emissions intensity and economic affluence reveals a critical equity concern for modern carbon pricing policy. Uniform carbon pricing—commonly implemented across cities—often places a disproportionate burden on lower-income communities and under-resourced small businesses already operating on thin margins, effectively penalizing rather than supporting those most in need of assistance. Rather than supporting an equitable transition, such one-size-fits-all approaches risk excluding the very actors most in need of assistance by imposing costs they are ill-equipped to bear, ultimately constraining their capacity to invest in energy-efficient upgrades. To advance a just and sustainable urban transition aligned with the Paris Agreement’s call to tailor climate action to local capacities [47], cities must design strategies that reflect local social and spatial disparities shaping both emissions and the ability to mitigate them [48, 49].

Our research enhances the contextual understanding of building operational carbon dynamics in cities by leveraging the increasing availability and quality of emerging open urban datasets. Notwithstanding, we highlight several caveats underlying our approach. Although we employ consistent citywide estimates of fuel and electricity intensities, the lack of high-resolution grid data limits the precision of our evaluations. Moreover, cities with a favorable overall energy mix may mask inefficiencies in building performance, highlighting the need to consider each city’s energy composition as a key lever for policy and infrastructure interventions. In addition, our analysis does not account for temporal trends in emissions, which could provide valuable insights into long-term decarbonization pathways. A further consideration is that our method relies on the availability of annual building energy data—which remains scarce or restricted in many cities. Even where such data exist, benchmarking laws may exclude portions of the building stock, introducing inherent modeling biases. Where building energy data are available, our approach transfers readily and adapts robustly to diverse data conditions in other cities. Recent policy shifts—such as new benchmarking mandates in Boston, Montréal, and Berlin, and expanded data-access initiatives in the UK—offer promising avenues to extend this work. For cities lacking building-level energy data, we demonstrate the feasibility of cross-city model training and the development of a unified model applicable across contexts. Building on this foundation, future research should aim to develop a global, task-specific urban model for estimating emissions in cities lacking building energy data. Lastly, the emergence of carbon hotspots beyond traditional urban cores suggests new opportunities for redefining city boundaries based on the spatial distribution of emissions [50]. Together, these advances can help close critical knowledge gaps and deepen the global understanding of urban carbon dynamics.

Methods

Our work introduces a graph deep learning model that integrates open data on building energy usage and crowdsourced geospatial information to predict building operating carbon at the city-scale. We apply our framework to multiple cities characterized by diverse geographical contexts and regional climates—Melbourne, New York (Manhattan), Seattle, Singapore, and Washington DC. Our method involves constructing one comprehensive city-scale graph for each city, encompassing all nodes and edge information. To overcome memory constraints associated with training on large graphs, we implement a graph sub-batching technique. This

approach involves sampling neighborhood subgraphs based on node indices, which are then iteratively utilized during model training.

Numerous studies show the importance of interactions between buildings and their neighbors in determining building energy performance [51, 52, 53, 54]. For instance, buildings within the same area may be subject to similar management policies or zoning regulations, and their proximity and morphological characteristics can influence urban heat island effects. We account for this relationship by explicitly modeling the structural connections between buildings and their urban context, which allows our model to better capture non-linear spatial relationships and enhances the accuracy of building energy predictions.

Measured Building Emissions

Our study uses reported site energy use data, which captures the total annual energy consumed by each building, including all energy sources—such as electricity from the grid, on-site renewables, fuel oil, propane, steam, and natural gas. In New York City, annual reported building energy data is accessed through the NYC OpenData portal (<https://opendata.cityofnewyork.us/>), specifically under the NYC Building Energy and Water Data Disclosure for Local Law of 2009 (LL84). Similarly, modeled building energy consumption data for Melbourne is obtained from the city's open data portal (<https://www.data.vic.gov.au/>), collected by the Commonwealth Scientific and Industrial Research Organization (CSIRO) under a liberal CC BY license. Seattle provides annual reported building energy data through its open data platform (<https://data.seattle.gov/>) as per the Seattle Energy Benchmarking Law. Washington DC's annual reported building energy data, mandated by the Clean and Affordable Energy Act of 2008, is accessible through (<https://opendata.dc.gov/>), collected annually by the Columbia Department of Energy and Environment (DOEE). Singapore's reported building energy data, obtained from the 2021 Building Energy Benchmarking Report (BEBR) by the Singapore Building Construction Authority (BCA), is released under the Singapore Open Data License (<https://beta.data.gov.sg/open-data-license/>). We enhance this dataset by incorporating residential building energy data obtained from two sources: the Singapore Housing and Development Board (HDB) and the real estate platform "99.co" (<https://www.99.co/singapore/>). Our estimation method employs a bottom-up approach that aggregates average consumption across various household types in each planning area.

Some cities provide total annual energy consumption data while other cities provide data in annual energy usage intensity (EUI). We obtain total annual energy consumption by multiplying EUI by the building's reported gross floor area (GFA). We then determine the annual operating carbon of each building by applying a constant carbon intensity of energy factor [55]. Energy mix is different across different cities, resulting in different carbon intensities. In the United States, energy-related CO₂ emissions are typically associated with fossil fuels (petroleum, natural gas, and coal). To address the significant variability in carbon intensities among American states [56], we use state-level carbon intensity of energy production factors sourced from the United States Energy Information Administration (EIA) (<https://www.eia.gov/environment/emissions/state/>). For each city, we apply the most up-to-date conversion factor available, measured in kilograms of CO₂ per kilowatt-hour—Melbourne (0.533034), New York (0.15559), Seattle (0.12079), Singapore (0.44876), and Washington DC (0.17470). Notably, we employ carbon intensity of electricity factors for Melbourne and Singapore, as the reported building EUI figures are reported in terms of electricity generation rates.

Since contextual features of building morphology are derived from OSM building footprints, it's crucial to link each building and its energy data to its corresponding OSM building entity. To achieve this linkage, we employ a two-step approach. First, we establish the spatial representation of buildings by utilizing their centroids or footprints. In cases where no spatial information is available, we utilize Google's Geocoding API to geocode each building and obtain its spatial location, although other geocoding APIs are also viable options. Subsequently, we match each building with its unique OSM building footprint identifier. It's important to note that the spatial matching process can be complex due to potential one-to-many and many-to-one relationships. To ensure one-to-one matching, we first check for self-overlapping instances between buildings polygons in both the OSM building and building energy benchmark datasets. This significantly reduces the occurrence of duplicate matches between subsets. Next we spatially overlay building polygons between the two building polygon sets and exclude buildings with multiple matches or no matches from further analysis. Supplementary Table 2 presents a comprehensive overview of the final energy benchmarking dataset along with carbon emission statistics for various building types.

Heterogeneous City Graph

Cities are complex systems with non-linear dynamics between urban elements [57]. To capture the non-linear relationship between buildings and their context, we represent the relational relationship through a heterogeneous graph of urban elements—buildings (B), urban plots (P), streets (S), and street intersections (I). Our network extends from the traditional primal planar network representation [58] where nodes and edges represent street intersections and non-intersecting street segments, integrating building and urban plot nodes as additional node types. Building nodes and plot nodes are derived from the representative points of their respective footprints. Edge relations between node types are determined by their proximity and topologic relationship to one another. For example, we define neighboring buildings as the three nearest neighbors by Euclidean distance between building centroids. Without loss of generality, we define a heterogeneous network as $G = \{N, E, R, T\}$:

$$n_i \subset N$$

$$n_i, r, n_j \subset E$$

$$T(n_i)$$

$$r \subset R$$

where N, E, R, T, refers to the set of nodes, set of edges, edge relation type, and node relation type respectively. In our case, node types correspond to $T = \{B, P, S, I\}$ and edge types $R = \{B_B, B_S, B_P, P_P, P_S, S_I\}$.

We employ the Urbanity Python package [59] to construct a richly attributed representation of each network node and its spatial connections. A comprehensive list of computed urban indicators is provided in Supplementary Table 1. Supplementary Table 3 summarizes the number of nodes and edges for each city.

Remote Sensing

High-resolution satellite and aerial imagery are sourced from Mapbox's global raster tile-set, which compiles imagery from multiple providers including NASA, USGS, Maxar, and Nearmaps (<https://docs.mapbox.com/help/glossary/mapbox-satellite/>). For each study area, we retrieve zoom level 19 image tiles encompassing the full urban extent.

Building-level satellite chips are extracted by locating each building’s centroid and isolating the corresponding pixels.

We incorporate Local Climate Zones (LCZs) [60], a global urban classification system that divides landscapes into 17 standardized urban and rural types based on physical and land cover attributes. Our analysis uses the 100-meter resolution global LCZ dataset [61], which is openly available under the CC BY 4.0 license. To capture LCZ heterogeneity, we compute Shannon entropy:

$$C_i = - \sum_{i=1}^K P(x_i)(\log_b P(x_i)) \quad (1)$$

where $P(x_i)$ is class probability for i-th class over K possible local climate zone categories.

We also incorporate global, scale-corrected estimates of real GDP per capita derived from 2019 nightlight data at 1-kilometer resolution [42].

To evaluate localized warming, we use the Urban Heat Island Indicator (UHII), which quantifies the average temperature difference between urban areas and their surrounding reference areas. Specifically, we employ global all-sky surface UHII estimates at 1-kilometer resolution, derived from the 2020 seamless all-sky land surface temperature product [62].

Crowdsourced Street View Images

We leverage imagery from Mapillary, a globally crowdsourced street-level image platform with extensive spatial coverage across cities. Licensed under CC BY-SA 4.0, Mapillary allows free use and adaptation, unlike proprietary alternatives. We apply spatial filtering to isolate city-level SVI and subsequently extract visual features through a segmentation pipeline [63].

Population Density Maps

To estimate population distribution, we use high-resolution (1-arcsecond) global population maps from Meta’s machine learning-derived datasets, which are trained on satellite imagery from Maxar [64]. Data is accessible via Humanitarian Data Exchange (HDX) and Amazon Web Services (AWS), available in both CSV and GeoTIFF formats.

Estimated Building Heights

Building height is a key variable for accurately modeling the relationship between urban density and carbon emissions. We use the global 3D building footprints dataset by [65], which estimates building heights by integrating multi-source remote sensing data with morphological features and machine learning. This dataset demonstrates robust predictive performance with reported R^2 values between 0.66 and 0.96 and root-mean-square errors (RMSE) ranging from 1.9 to 14.6 meters across 33 subregions. Additionally, the selected dataset closely aligns with manually validated reference datasets provided by established entities such as ONEGEO Map, Baidu Maps, the United States Geological Survey (USGS), Microsoft Building Heights, and EMU Analytics (England).

OpenStreetMap

OpenStreetMap (OSM) provides foundational geospatial layers, including roads, building footprints, and points of interest. The data, distributed under the Open Database License (ODbL), is accessed through the Pyrosm API, which pulls regularly updated extracts from GeoFabrik. For analysis, we: (1) simplify road networks into planar graphs, (2) validate and relabel points of interest, and (3) ensure that building footprints are converted into valid polygon geometries.

Multi-Modal Model Architecture

Our prediction task involves node-level graph regression, specifically aiming to predict building operating carbon emissions using multi-modal geospatial data, including aerial and street-view imagery as well as tabular features such as population counts, points-of-interest (POI) categories, and road network characteristics.

To achieve this, we design an end-to-end deep learning architecture comprising two primary modules: an aerial imagery branch and a graph convolution branch. The aerial imagery branch processes top-down building images using a ResNet-50 backbone, generating 1000-dimensional embedding which we then pass to a 128-dimensional fully connected layer. Simultaneously, the graph convolutional branch employs a two-layer heterogeneous GraphSAGE model [66] which integrates building features (16 dimensions), plot features (45 dimensions), street features (11 dimensions), and intersection features (8 dimensions).

To capture the multifaceted ways in which the urban context can influence building emissions, we compute a comprehensive set of urban analytical features encompassing network topology, building and plot morphology, street view indicators, local climate zones, population density, and urban points of interest. Studies have demonstrated that street view features are strongly linked to pedestrian thermal comfort and the urban heat island effect—both of which affect buildings’ cooling loads [67]. Similarly, street network metrics and points of interest (e.g., street intersection centrality and the availability of urban services) have been consistently associated with building energy profiles [68]. Urban form factors—such as local climate zones [60] and building morphology [69]—influence key building characteristics, including use intensity and land use interactions, all of which play critical roles in shaping building energy consumption.

Each GraphSAGE layer aggregates information from neighboring nodes based on adjacency relationships to produce a 128-dimensional embedding. We extract the final building node 128-dimensional embedding and 128-dimensional aerial imagery embedding and concatenate them into combined 256-dimensional feature vector, which is passed through two fully connected 1024-dimensional layers to produce the final prediction of building operating carbon emissions.

For model training and evaluation, we shuffle and split our dataset into training (70%), validation (15%), and test (15%) subsets. To evaluate and mitigate the risk of spatial data leakage, we conduct a k-nearest neighbor (kNN) regression analysis, comparing a model using only spatial coordinates with one using the full set of independent variables. The results (see Supplementary Table 4) indicate that predictive performance is not driven by spatial proximity or building similarity, supporting the robustness of our data split. Explanatory features are standardized, and a logarithmic transformation is applied to the target variable to handle the skewed distribution of building energy measurements. All model configurations are trained for 50 epochs with hyperparameter tuning across graph feature embedding sizes (64, 128, 256), learning rates (10^{-3} , 10^{-4} , 10^{-5}), and batch sizes (16, 32, 64). We utilize the Adam optimizer with default beta parameters (0.9, 0.999). During training, masks are applied to prevent message passing and aggregation from validation and test nodes. All models are implemented using the PyTorch Geometric deep learning framework [70]. We select the best-performing model based on the lowest mean squared logarithmic error (MSLE) to predict building operating carbon emissions across all buildings. We train and evaluate our models with one NVIDIA RTX 4090 GPU running on Ubuntu operating platform.

Baseline Benchmarking and Feature Ablation

To demonstrate the effectiveness of our proposed model architecture and multi-modal feature sets for building energy prediction, we evaluate model performance on various input feature combinations and machine learning algorithms, as detailed in Supplementary Table 5.

Our feature ablation study shows that building form features—such as height, footprint area, and volume—are the strongest predictors across models. Machine learning models rely heavily on these features and show little performance loss when other inputs are removed, indicating limited capacity to learn from more complex contextual data like POIs or street networks. In contrast, deep learning models remain robust even without building form data and perform especially well when using satellite imagery. This aligns with previous findings that satellite imagery is valuable for capturing urban-scale building emission patterns. These results point to a trade-off: machine learning models are efficient when building data is available, but deep learning models offer greater flexibility and generalization across varied urban contexts by learning complex and non-linear spatial connections.

We maintain a consistent data split across both the feature ablation study and benchmarking experiments to ensure comparability of performance. An additional goal of the feature ablation study is to identify the minimal subset of features required to achieve robust predictive performance, thus supporting practical applications in cities where data availability is limited.

Error Analysis of Model Uncertainty

To support interpretation of model findings and robustness, we quantify prediction uncertainty at the urban scale. As shown in Supplementary Figure 1, our model demonstrates robust performance, with low average errors across different groups of buildings in each city, supporting its consistency in estimating building emissions at the urban scale. We further validate our building-level emissions estimates by examining their correlation with real GDP per capita at the urban scale. Our findings align with empirical studies [71] and demonstrate strong correlations between predicted emissions and real GDP per capita in Melbourne ($R = 0.519$, $p < 0.001$), NYC-Manhattan ($R = 0.459$, $p < 0.001$), Seattle ($R = 0.717$, $p < 0.001$), Singapore ($R = 0.787$, $p < 0.001$), Washington DC ($R = 0.459$, $p < 0.001$), and across all cities combined ($R = 0.457$, $p < 0.001$). The linear scaling of urban emissions with GDP per capita at high spatial resolution highlights the strong alignment between our model predictions and socioeconomic patterns at the urban scale. Supplementary Figure 2 illustrates the spatial association between building emissions and GDP per capita within 1 km grid cells, highlighting how emissions patterns mirror economic activity at finer spatial scales.

Cross-city Model Performance

Against the trend of task-specific urban foundation models, we explored the feasibility of training a combined model across multiple cities. Our cross-city approach yielded promising results—Melbourne (RMSE = 0.670, $R^2 = 0.835$); NYC-Manhattan (RMSE = 0.738, $R^2 = 0.550$); Seattle (RMSE = 0.758, $R^2 = 0.507$); Singapore (RMSE = 0.590, $R^2 = 0.680$); Washington DC (RMSE = 0.868, $R^2 = 0.377$). Overall, the cross-city model demonstrates strong performance, explaining 78.4% of the variance across all cities with a root mean squared error (RMSE) of 0.699. Although the cross-city model performance do not exceed the city-specific models, it shows the possibility of training a global, task-specific urban foundation model for building energy prediction with our approach. Notably, a primary drawback we noticed with the cross-city approach was the significantly increased computational demand: the model required more than twice as many training epochs as the city-specific models to reach a learning saturation point.

Data Availability

The datasets in this study are publicly available as follows or can be obtained from Google Earth Engine. The benchmarking mandate data for each city is available at: Melbourne (<https://discover.data.vic.gov.au/dataset/property-level-energy-consumption-modelled-on-building-attributes-baseline-2011-and-b-2016-2026>), NYC (<https://data.cityofnewyork.us/d/5zyy-y8am>), Seattle (<https://data.seattle.gov/d/teqw-tu6e>), Singapore (<https://www1.bca.gov.sg/buildsg/sustainability/regulatory-requirements-for-existing-buildings/bca-building-energy-benchmarking-and-disclosure>), and Washington DC (<https://opendata.dc.gov/maps/10f4f09fc5684d9988ae83ae4cca8b70>). The OpenStreetMap daily data extracts are available at <https://www.geofabrik.de/data/download.html>. The crowdsourced street view imagery can be obtained via Mapillary API with a registered developer key at: <https://www.mapillary.com/developer/api-documentation>. Users can register for a Mapbox satellite imagery API access key at: (<https://docs.mapbox.com/help/glossary/mapbox-satellite/>). Global 3-D Building Footprint are available at: Americas, Africa, and Oceania (<https://zenodo.org/records/15459025>), Asia (<https://doi.org/10.5281/zenodo.11397014>), and Europe (<https://doi.org/10.5281/zenodo.11391076>). The Meta High Resolution Population Density Maps are available at https://data.humdata.org/organization/meta?dataseries_name=Data+for+Good+at+Meta+-+High+Resolution+Population+Density+Maps+and+Demographic+Estimates. The Global Map of Local Climate Zone is available under Google Earth Engine API at: https://developers.google.com/earth-engine/datasets/catalog/RUB_RUBCLIM_LCZ_global_lc_map_latest

Code and Software Availability

The analysis was conducted using Python. We provide accompanying datasets, download instructions, and source code at the project GitHub repository (<https://github.com/winstonyym/open-building-energy-prediction>).

Acknowledgements

We thank the members of the NUS Urban Analytics Lab for the discussions. W.Y. thankfully acknowledges the NUS Graduate Research Scholarship granted by the National University of Singapore. This research is part of the project Large-scale 3D Geospatial Data for Urban Analytics, which is supported by the National University of Singapore under the Start-Up Grant R-295-000-171-133.

Author Contributions

Winston Yap 1) Methodology Conceptualization and Design; 2) Conceive study; 3) Methodology Development; 4) Data Acquisition and Analysis; 5) Data Testing and Validation; 6) Wrote Original Manuscript.

Abraham Noah Wu 1) Methodology Conceptualization and Design; 2) Conceive study; 3) Revise and Review Manuscript.

Clayton Miller 1) Methodology Conceptualization and Design; 2) Revise and Review Manuscript.

Filip Biljecki 1) Methodology Conceptualization and Design; 2) Revise and Review Manuscript; 3) Research Supervision; 4) Project Funding.

Competing Interests

The authors declare no competing financial or non-financial interests.

References

- [1] Tong, D. *et al.* Committed emissions from existing energy infrastructure jeopardize 1.5 °C climate target. *Nature* **572**, 373–377 (2019).
- [2] Intergovernmental Panel on Climate Change. Global warming of 1.5 °C (2018).
- [3] International Energy Agency. Tracking clean energy progress 2023 (2023).
- [4] Hsu, A. *et al.* Climactor, harmonized transnational data on climate network participation by city and regional governments. *Scientific Data* **7**, 374 (2020).
- [5] John, L. *et al.* Net zero stocktake 2023 (2023).
- [6] International Energy Agency. Buildings (2023).
- [7] Riahi, K. *et al.* Mitigation pathways compatible with long-term goals (2022).
- [8] Arias, P. *et al.* Climate change 2021: the physical science basis. contribution of working group i to the sixth assessment report of the intergovernmental panel on climate change; technical summary (2021).
- [9] Intergovernmental Panel on Climate Change & Intergovernmental Panel on Climate Change. Human Settlements, Infrastructure, and Spatial Planning. in Climate Change 2014 Mitigation of Climate Change (2015).
- [10] Hsu, A., Wang, X., Tan, J., Toh, W. & Goyal, N. Predicting european cities' climate mitigation performance using machine learning. *Nature Communications* **13**, 7487 (2022).
- [11] Ribeiro, H. V., Rybski, D. & Kropp, J. P. Effects of changing population or density on urban carbon dioxide emissions. *Nature communications* **10**, 3204 (2019).
- [12] Güneralp, B. *et al.* Global scenarios of urban density and its impacts on building energy use through 2050. *Proceedings of the National Academy of Sciences* **114**, 8945–8950 (2017).
- [13] Barrington-Leigh, C. & Millard-Ball, A. Global trends toward urban street-network sprawl. *Proceedings of the National Academy of Sciences* **117**, 1941–1950 (2020).
- [14] Georgescu, M., Morefield, P. E., Bierwagen, B. G. & Weaver, C. P. Urban adaptation can roll back warming of emerging megapolitan regions. *Proceedings of the National Academy of Sciences* **111**, 2909–2914 (2014).
- [15] Berrill, P., Wilson, E. J., Reyna, J. L., Fontanini, A. D. & Hertwich, E. G. Decarbonization pathways for the residential sector in the united states. *Nature Climate Change* **12**, 712–718 (2022).
- [16] Shao, M., Wang, X., Bu, Z., Chen, X. & Wang, Y. Prediction of energy consumption in hotel buildings via support vector machines. *Sustainable Cities and Society* **57**, 102128 (2020).
- [17] World Economic Forum. To create net-zero cities, we need to look hard at our older buildings (2022).
- [18] Zhao, X., Yin, Y., Zhang, S. & Xu, G. Data-driven prediction of energy consumption of district cooling systems (dcs) based on the weather forecast data. *Sustainable Cities and Society* **90**, 104382 (2023).
- [19] Reinhart, C. F. & Davila, C. C. Urban building energy modeling—a review of a nascent field. *Building and Environment* **97**, 196–202 (2016).
- [20] Howard, B. *et al.* Spatial distribution of urban building energy consumption by end use. *Energy and buildings* **45**, 141–151 (2012).
- [21] Mohammadi, N. & Taylor, J. E. Urban energy flux: Spatiotemporal fluctuations of building energy consumption and human mobility-driven prediction. *Applied energy* **195**, 810–818 (2017).
- [22] Yang, Y., Tan, Z. & Schläpfer, M. Assessing the space-use efficiency of french cities by coupling city volumes with mobile data traffic. *Sustainable Cities and Society* **124**, 106292 (2025).
- [23] Hong, T., Chen, Y., Luo, X., Luo, N. & Lee, S. H. Ten questions on urban building energy modeling. *Building and Environment* **168**, 106508 (2020).
- [24] Chou, J.-S. & Tran, D.-S. Forecasting energy consumption time series using machine learning techniques based on usage patterns of residential householders. *Energy* **165**, 709–726 (2018).
- [25] Streltsov, A., Malof, J. M., Huang, B. & Bradbury, K. Estimating residential building energy consumption using overhead imagery. *Applied Energy* **280**, 116018 (2020).
- [26] Dougherty, T. R., Huang, T., Chen, Y., Jain, R. K. & Rajagopal, R. Schmear: scalable construction of holistic models for energy analysis from rooftops. In *Proceedings of the 8th ACM International Conference on Systems for Energy-Efficient Buildings, Cities, and Transportation*, 111–120 (2021).
- [27] Biljecki, F. & Ito, K. Street view imagery in urban analytics and gis: A review. *Landscape and Urban Planning* **215**, 104217 (2021).

- [28] Biljecki, F., Zhao, T., Liang, X. & Hou, Y. Sensitivity of measuring the urban form and greenery using street-level imagery: A comparative study of approaches and visual perspectives. *International Journal of Applied Earth Observation and Geoinformation* **122**, 103385 (2023).
- [29] Zhang, F. *et al.* Urban visual intelligence: Studying cities with artificial intelligence and street-level imagery. *Annals of the American Association of Geographers* 1–22 (2024).
- [30] Sun, M. *et al.* Understanding building energy efficiency with administrative and emerging urban big data by deep learning in glasgow. *Energy and Buildings* **273**, 112331 (2022).
- [31] Mayer, K. *et al.* Estimating building energy efficiency from street view imagery, aerial imagery, and land surface temperature data. *Applied Energy* **333**, 120542 (2023).
- [32] Sun, M. & Bardhan, R. Identifying hard-to-decarbonize houses from multi-source data in cambridge, uk. *Sustainable Cities and Society* **100**, 105015 (2024).
- [33] Yap, W. & Biljecki, F. A global feature-rich network dataset of cities and dashboard for comprehensive urban analyses. *Scientific Data* **10**, 667 (2023).
- [34] Hou, Y. *et al.* Global streetscapes – a comprehensive dataset of 10 million street-level images across 688 cities for urban science and analytics. *ISPRS Journal of Photogrammetry and Remote Sensing* **215**, 216–238 (2024).
- [35] Goldstein, B., Gounaris, D. & Newell, J. P. The carbon footprint of household energy use in the united states. *Proceedings of the National Academy of Sciences* **117**, 19122–19130 (2020).
- [36] de Chalendar, J. A., Taggart, J. & Benson, S. M. Tracking emissions in the us electricity system. *Proceedings of the National Academy of Sciences* **116**, 25497–25502 (2019).
- [37] World Economic Forum. To meet our global climate ambitions, we must tackle embodied carbon (2024).
- [38] Global Alliance for Buildings and Construction. 2021 global status report for buildings and construction (2021).
- [39] of Climate, N. M. O. & Justice, E. Buildings (2024). URL <https://climate.cityofnewyork.us/subtopics/buildings/>.
- [40] Timmons, D., Zirogiannis, N. & Lutz, M. Location matters: Population density and carbon emissions from residential building energy use in the united states. *Energy research & social science* **22**, 137–146 (2016).
- [41] Gudipudi, R., Fluschnik, T., Ros, A. G. C., Walther, C. & Kropp, J. P. City density and co2 efficiency. *Energy Policy* **91**, 352–361 (2016).
- [42] Chen, J. *et al.* Global 1 km× 1 km gridded revised real gross domestic product and electricity consumption during 1992–2019 based on calibrated nighttime light data. *Scientific Data* **9**, 202 (2022).
- [43] Fox, S., Agyemang, F., Hawker, L. & Neal, J. Integrating social vulnerability into high-resolution global flood risk mapping. *Nature communications* **15**, 3155 (2024).
- [44] Jaganathan, S. *et al.* Estimating the effect of annual pm_{2·5} exposure on mortality in india: a difference-in-differences approach. *The Lancet Planetary Health* **8**, e987–e996 (2024).
- [45] Creutzig, F., Baiocchi, G., Bierkandt, R., Pichler, P.-P. & Seto, K. C. Global typology of urban energy use and potentials for an urbanization mitigation wedge. *Proceedings of the national academy of sciences* **112**, 6283–6288 (2015).
- [46] Jones, C. & Kammen, D. M. Spatial distribution of us household carbon footprints reveals suburbanization undermines greenhouse gas benefits of urban population density. *Environmental science & technology* **48**, 895–902 (2014).
- [47] United Nations Framework Convention on Climate Change. The paris agreement (2015).
- [48] Moore, F. C. *et al.* Determinants of emissions pathways in the coupled climate–social system. *Nature* **603**, 103–111 (2022).
- [49] Yu, Y. *et al.* Decarbonization efforts hindered by china's slow progress on electricity market reforms. *Nature Sustainability* **6**, 1006–1015 (2023).
- [50] Dong, L. *et al.* Defining a city—delineating urban areas using cell-phone data. *Nature Cities* **1**, 117–125 (2024).
- [51] Pisello, A. L., Taylor, J. E., Xu, X. & Cotana, F. Inter-building effect: Simulating the impact of a network of buildings on the accuracy of building energy performance predictions. *Building and environment* **58**, 37–45 (2012).
- [52] Li, Y., Schubert, S., Kropp, J. P. & Rybski, D. On the influence of density and morphology on the urban heat island intensity. *Nature communications* **11**, 2647 (2020).
- [53] Gao, J. & Bukovsky, M. S. Urban land patterns can moderate population exposures to climate extremes over the 21st century. *Nature Communications* **14**, 6536 (2023).
- [54] Hou, H., Su, H., Yao, C. & Wang, Z.-H. Spatiotemporal patterns of the impact of surface roughness and morphology on urban heat island. *Sustainable Cities and Society* **92**, 104513 (2023).

- [55] Ritchie, H., Roser, M. & Rosado, P. Co₂ and greenhouse gas emissions. *Our world in data* (2020).
- [56] Hsu, A., Sheriff, G., Chakraborty, T. & Manya, D. Disproportionate exposure to urban heat island intensity across major us cities. *Nature communications* **12**, 2721 (2021).
- [57] Batty, M. *Cities as Complex Systems: Scaling, Interaction, Networks, Dynamics and Urban Morphologies*. (Springer, 2009).
- [58] Barthélémy, M. Spatial networks. *Physics reports* **499**, 1–101 (2011).
- [59] Yap, W., Stouffs, R. & Biljecki, F. Urbanity: automated modelling and analysis of multidimensional networks in cities. *npj Urban Sustainability* **3** (2023).
- [60] Stewart, I. D. & Oke, T. R. Local climate zones for urban temperature studies. *Bulletin of the American Meteorological Society* **93**, 1879–1900 (2012).
- [61] Demuzere, M. *et al.* A global map of local climate zones to support earth system modelling and urban scale environmental science. *Earth System Science Data Discussions* **2022**, 1–57 (2022).
- [62] Yang, Q. *et al.* A global urban heat island intensity dataset: Generation, comparison, and analysis. *Remote Sensing of Environment* **312**, 114343 (2024).
- [63] Cheng, B., Misra, I., Schwing, A. G., Kirillov, A. & Girdhar, R. Masked-attention mask transformer for universal image segmentation. In *Proceedings of the IEEE/CVF Conference on Computer Vision and Pattern Recognition*, 1290–1299 (2022).
- [64] Facebook Connectivity Lab and Center for International Earth Science Information Network - CIESIN - Columbia University. High resolution settlement layer (hrs1). ((2016)). Source imagery for HRS1 © 2016 DigitalGlobe. Accessed 1 Aug 2023.
- [65] Che, Y. *et al.* 3d-globfp: The first global three-dimensional building footprint dataset. *Earth System Science Data Discussions* **2024**, 1–28 (2024).
- [66] Hamilton, W., Ying, Z. & Leskovec, J. Inductive representation learning on large graphs. *Advances in Neural Information Processing Systems* **30** (2017).
- [67] Yang, S., Chong, A., Liu, P. & Biljecki, F. Thermal comfort in sight: Thermal affordance and its visual assessment for sustainable streetscape design. *Building and Environment* 112569 (2025).
- [68] Song, C. *et al.* Developing urban building energy models for shanghai city with multi-source open data. *Sustainable Cities and Society* **106**, 105425 (2024).
- [69] Biljecki, F. & Chow, Y. S. Global building morphology indicators. *Computers, Environment and Urban Systems* **95**, 101809 (2022).
- [70] Fey, M. & Lenssen, J. E. Fast graph representation learning with pytorch geometric (2019). Preprint at <https://arxiv.org/abs/1903.02428>
- [71] Institute, E. Statistical review of world energy (2024). URL <https://www.energyinst.org/statistic/al-review>.